Tungsten Phosphide Nanorod Arrays Directly Grown on Carbon Cloth: A Highly Efficient and Stable Hydrogen Evolution Cathode at All pH Values

Zonghua Pu,[†] Qian Liu,[†] Abdullah M. Asiri,[§,‖] and Xuping Sun*[,†,§,‖]

[†]Chemical Synthesis and Pollution Control Key Laboratory of Sichuan Province, School of Chemistry and Chemical Engineering, China West Normal University, Nanchong 637002, Sichuan, China

[§]Chemistry Department, Faculty of Science, and [‖]Center of Excellence for Advanced Materials Research, King Abdulaziz University, Jeddah 21589, Saudi Arabia

S *Supporting Information*

ABSTRACT: We report the development of tungsten phosphide nanorod arrays on carbon cloth (WP NAs/CC) through a two-step strategy: hydrothermally growing WO_3 nanorod arrays on CC (WO_3 NAs/CC) first, followed by phosphidation to chemically convert the WO_3 NAs/CC precursor into WP NAs/CC. As a novel integrated 3D hydrogen evolution cathode in acidic media, the WP NAs/CC electrode exhibits excellent catalytic activity and durability. It needs overpotentials of 130 and 230 mV to afford current densities of 10 and 100 mA cm^{-2}, respectively, and its catalytic activity is maintained for at least 70 h. Remarkably, this electrode also works efficiently in both neutral and alkaline solutions.
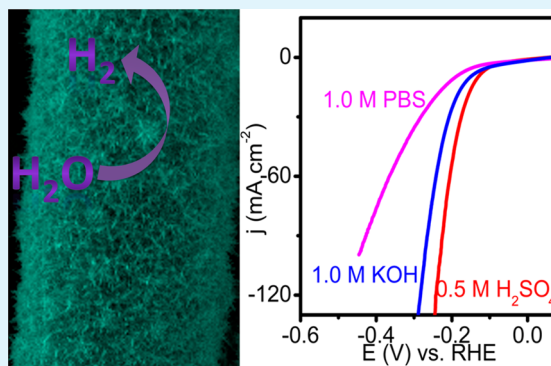
KEYWORDS: *tungsten phosphide, nanorod arrays, hydrogen evolution cathode, all pH values, water splitting*

Cost-effective, sustainable, and efficient hydrogen production is required for the vision of using hydrogen as a future clean energy carrier.[1] Electrochemical water splitting offers a simple route for large-scale production of highly pure hydrogen. An efficient hydrogen evolution reaction (HER) electrocatalyst is usually needed for achieving large cathodic current densities at low overpotentials.[2] Water electrolysis units based on proton exchange membrane (PEM) technology operate under strongly acidic conditions,[3] and many solar water-splitting devices are designed to work under acidic conditions.[4] Although platinum-based materials are the best HER catalyst, their widespread use is limited because of their high cost. Abundant nickel-based alloys have been largely developed as efficient HER catalysts, but they suffer from corrosion stability in acidic media. Developing acid-stable non-noble-metal HER catalysts is thus highly attractive and would represent a significant step to facilitate the transition to hydrogen economy.[5] Molybdenum-based compounds are one big family of such catalysts receiving great research attention in recent years, including MoS_2,[6] Mo_2C,[7] MoB,[7] $NiMoN_x/C$,[8] and $Co_{0.6}Mo_{1.4}N_2$,[9] etc. On the other hand, microbial electrolysis cell offers a biological route to hydrogen production but needs catalysts operating under neutral conditions[10] and alkaline electrolysis is an attractive alternative to PEM-based electrolysis but requires using catalysts efficiently in alkaline media.[11] Accordingly, the design of HER catalysts capable of operating efficiently at all pH values is highly desired but still remains challenging, and only very few such catalysts have been reported so far, including CoP/CC[12] and Co-NRCNTs.[13]

Tungsten, belonging to the same group with molybdenum, is also emerging as another interesting non-noble metal for its electrocatalytic ability toward hydrogen evolution. Although tungsten carbides are active HER catalysts in acidic media, they suffer from limited corrosion stability under neutral and higher pH conditions.[14] W_2N nanowires exhibit improved stability, but they need a large overpotential (η) of 500 mV to afford current density of 10 mA cm^{-2}.[15] Considerable efforts has also been made to develop WS_2-based HER catalysts with attractive activity;[16] however, WS_2 suffers from poor electrical conductivity and works well only in acidic media. Obviously, an ideal HER electrocatalyst should have good electrical conductivity to enhance electronic transfer.[6] Transition metal phosphides (TMPs) have good electrical conductivity and thus satisfy this requirement. Several TMPs like including Ni_2P,[17] CoP,[12,18] FeP,[19] and MoP[20] have recently been developed by us and other researchers as efficient catalysts for electro-chemical hydrogen evolution. More recently, amorphous WP nanoparticles have been developed as an efficient HER catalyst operating in acidic solutions.[21]
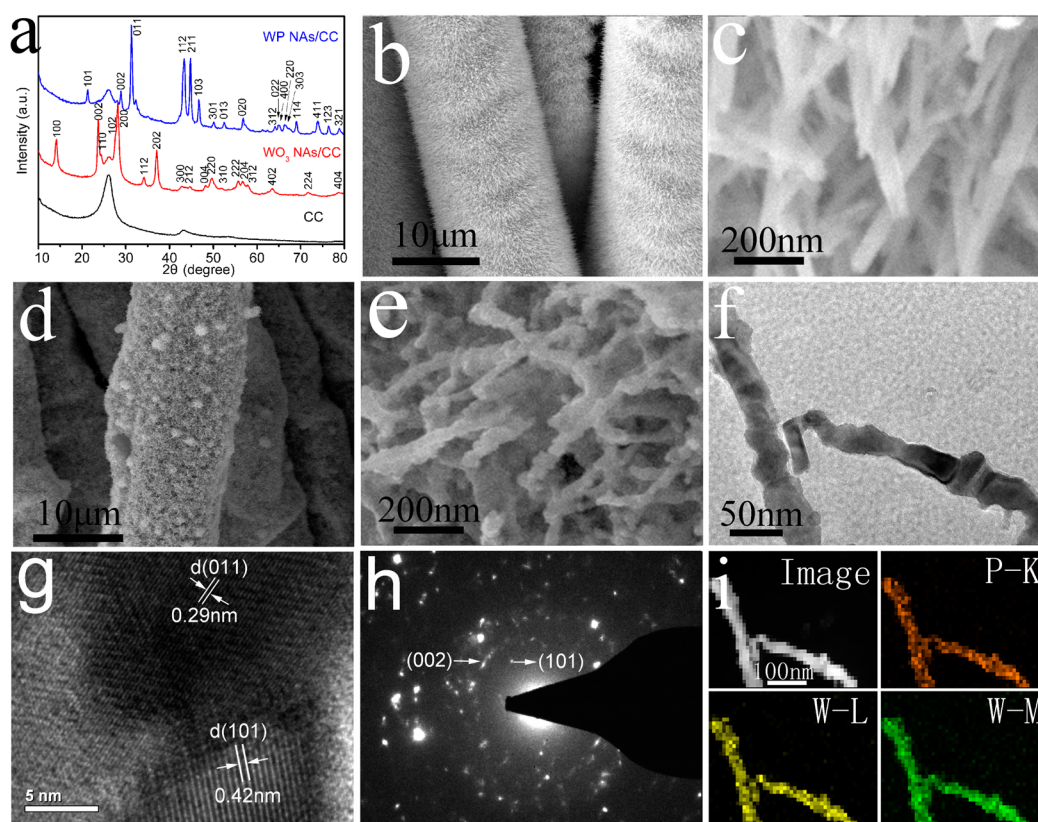
Figure 1. (a) XRD patterns for CC, WO$_3$ NAs/CC, and WP NAs/CC. (b, c) SEM images of WO$_3$ NAs/CC. (d, e) SEM images of WP NAs/CC. (f) TEM image of the WP nanorods. (g) HRTEM image (The zone axis is [11$\bar{1}$]) and (h) SAED pattern taken from one single WP nanorod. (i) STEM image and EDX elemental mapping of P and W for the WP nanorods.

Prior to electrochemical tests, however, most reported HER catalysts are required to be effectively immobilized on current collectors with the use of a polymer binder like Nafion or PTFE as a film-forming agent. The polymer binder generally increases the series resistance[22] and may block active sites and inhibit diffusion leading to reduced effective catalytic activity.[23] Our recent work demonstrates that the direct growth of the active phases on the current collectors can lead to an efficient integrated hydrogen evolution cathode with intimate contact, good mechanical adhesion, and excellent electrical connection between these two components.[12]

In this work, we describe our recent effort toward this direction in developing tungsten phosphide nanorod arrays on carbon cloth (WP NAs/CC) through a two-step strategy: hydrothermally growing WO$_3$ nanorod arrays on CC (WO$_3$ NAs/CC) first, followed by phosphidation to chemically convert the WO$_3$ NAs/CC precursor into WP NAs/CC. The WP NAs/CC, as an integrated hydrogen evolution cathode, exhibits excellent catalytic activity and durability in acidic media. It needs overpotentials of 130 and 230 mV to afford current densities of 10 and 100 mA cm^{-2}, respectively, and its catalytic activity is preserved for at least 70 h. Notably, this electrode also works efficiently in both neutral and alkaline solutions. The WP NAs/CC offers us an efficient cost-effective 3D cathode toward electrochemical water splitting for large-scale hydrogen fuel production under all pH conditions.

The X-ray diffraction (XRD) patterns for WO$_3$ NAs/CC and WP NAs/CC are shown in Figure 1a. The WO$_3$ NAs/CC shows diffraction peaks characteristic of hexagonal-phase WO$_3$ (JCPDS No. 85−2460). After phosphidation, only peaks

corresponding to orthorhombic WP are observed (JCPDS No. 29−1364). For both samples, the strong peaks at 26° and 43° are assigned to the CC substrate. Figure 1b, c shows the scanning electron microscopy (SEM) images of WO$_3$ NAs/CC, revealing the surface of each carbon fiber is fully covered with WO$_3$ nanorod arrays. Following phosphidation, the 1D morphology is still maintained (Figure 1d, e). The corresponding energy dispersive X-ray (EDX) spectrum (see Figure S1 in the Supporting Information) shows that the atomic ratio between P and W is close to 1:1. The transmission electron microscopy (TEM) image of WP nanorods scratched down from CC shows that they have a diameter in the range of 30−50 nm, as shown in Figure 1f. The high-resolution TEM (HRTEM) image taken from one WP nanorod (Figure 1g) reveals clear lattice fringes with interplanar distances of 0.29 nm and 0.42 nm corresponding to the (011) and (101) planes of the orthorhombic WP, respectively. The selected area electron diffraction (SAED) pattern (Figure 1h) shows discrete spots indexed to the (101) and (002) planes of orthorhombic WP structure. Figure 1i shows the scanning TEM (STEM) and corresponding EDX elemental mapping images, further indicating both P and W elements are uniformly distributed throughout the whole nanorod. All these observations provide strong evidence to support the successful chemical conversion of WO$_3$ NAs/CC into WP NAs/CC after phosphidation reaction. Also note that the same preparation without the presence of CC only gives individual WO$_3$ nanorods (WO$_3$ NRs) and the subsequent phosphidation leads to WP nanorods (WP NRs) (see Figure S2 in the Supporting Information).
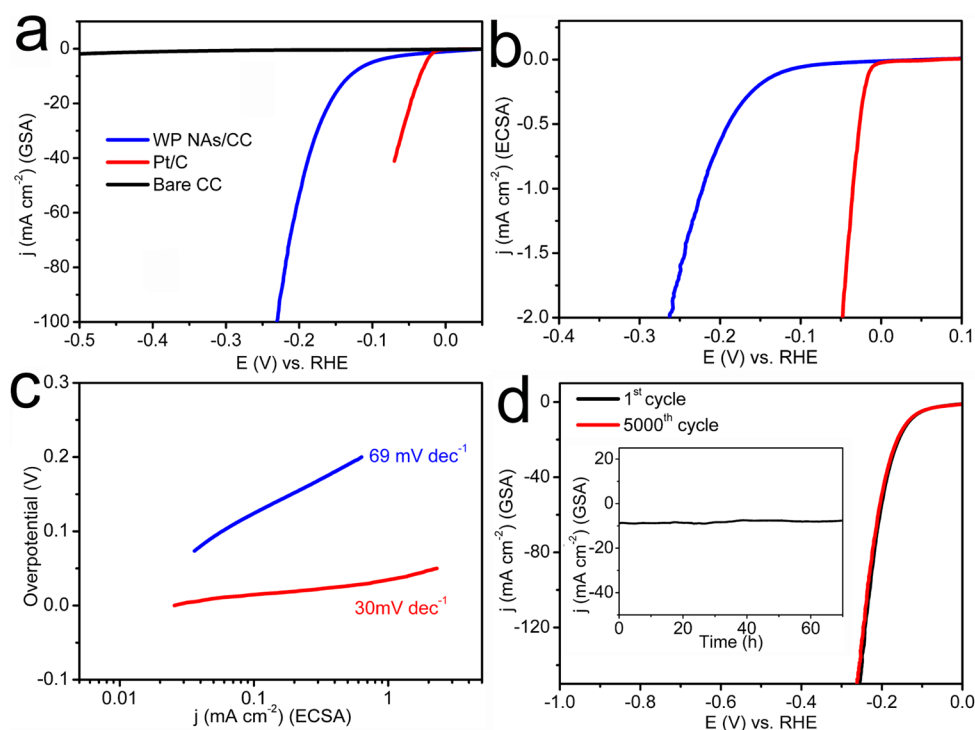
Figure 2. (a) Polarization curves for WP NAs/CC, Pt/C, and bare CC in 0.5 M H_2SO_4 with a scan rate of 2 mV s^{-1} with current density normalized by GSA of the electrodes. (b) Polarization curves and (c) Tafel plots for WP NAs/CC and Pt/C with current density normalized by ECSA. (d) Polarization curves for WP NAs/CC initial and after 5000 CV scanning between +0.28 and −0.27 V vs RHE (inset: time-dependent current density curve for WP NAs/CC under static overpotential of 120 mV for 70 h).

We directly applied the WP NAs/CC (WP loading: 2.0 mg cm^{-2}) as a hydrogen evolution cathode to highlight the merits of the unique architecture. Bare CC and commercial Pt/C deposited on CC were also tested as a comparison. A resistance test was made and *iR* compensation was applied for all the electrochemical measurements. Figure 2a show the polarization curves in 0.5 M H_2SO_4 with a scan rate of 2 mV s^{-1} with current density normalized by geometric surface area (GSA) (1 × 1 cm^2) of these electrodes. Pt/C catalyst exhibits expected HER activity with a near zero overpotential. Although bare CC shows negligible HER activity, the WP NAs/CC electrode is highly active toward the HER over this range of electrode potentials, implying the high activity of this electrode arises from WP. The onset of hydrogen evolution reaction is observed at around 50 mV, beyond which the cathodic current rises rapidly as more negative potential is applied. Moreover, this electrode needs overpotentials of 130 and 230 mV to afford current densities of 10 and 100 mA cm^{-2}, respectively. These overpotentials compare favorably to the values of most reported non-noble-metal HER catalysts in acidic media (see Table S1 in the Supporting Information). Figure 2b shows the replotted polarization curves for WP NAs/CC and Pt/C using the measured current normalized by the electrochemical active surface area (ECSA), and Figure 2c shows the corresponding Tafel plots recorded with the linear regions fitted into the Tafel equation ($\eta = a + b \log j$, where *b* is the Tafel slope and *j* is the current density). The Tafel slope of 30 mV dec^{-1} for Pt/C is consistent with the reported value.[12] The WP NAs/CC exhibits a Tafel slope of 69 mV dec^{-1} in the region of $\eta = 100-200$ mV, implying hydrogen evolution occurs through a Volmer-Heyrovsky mechanism.[24] The value of exchange current density of WP NAs/CC is calculated to be 0.29 mA cm^{-2} by extrapolating the Tafel plot (see Figure S4 in the Supporting

Information), which is the largest among all non-Pt HER catalysts listed in Table S1 in the Supporting Information.

It is of importance to mention that WP NRs immobilized on CC using Nafion (WP NRs/CC) is also electrochemically active toward the HER (WP loading: 2.0 mg cm^{-2}), as shown in Figure S5 in the Supporting Information. But to afford current density of 10 mA cm^{-2}, this electrode needs an overpotential of 173 mV, much larger than the value (130 mV) for WP NAs/CC. In addition, the WP NRs/CC also shows a higher Tafel slope (75 mV dec^{-1}) than WP NAs/CC (69 mV dec^{-1}). Durability was probed by continuous cyclic voltammetric (CV) sweeping of the WP NAs/CC electrode between +0.28 and −0.27 V vs RHE with a scan rate of 100 mV s^{-1} in 0.5 M H_2SO_4. Clearly, at the end of 5000 CV cycles, this electrode shows similar polarization curve to the initial one with negligible loss in current density (Figure 2d). The long-term stability of this electrode was also evaluated by electrolysis at a fixed overpotential of 120 mV, suggesting no performance degradation was observed after electrolysis for more than 70 h (inset). These results confirm the exceptional durability of this hydrogen evolution cathode.

We further studied the HER performance of the WP NAs/CC in 1.0 M PBS (pH 7). This electrode exhibits an onset overpotential of 100 mV and strong durability (Figure 3a). To afford a current density of 10 mA cm^{-2}, the WP NAs/CC needs an overpotential of 200 mV. This overpotential still compares favorably to the behavior of most reported Pt-free HER catalysts in neutral solutions (see Table S2 in the Supporting Information). Figure 3b shows the replotted polarization curve for WP NAs/CC using the measured current normalized by the ECSA, and the Tafel slope is 125 mV dec^{-1} calculated from the Tafel plot (Figure 3c). Note that the WP NAs/CC also performs well with excellent durability under alkaline
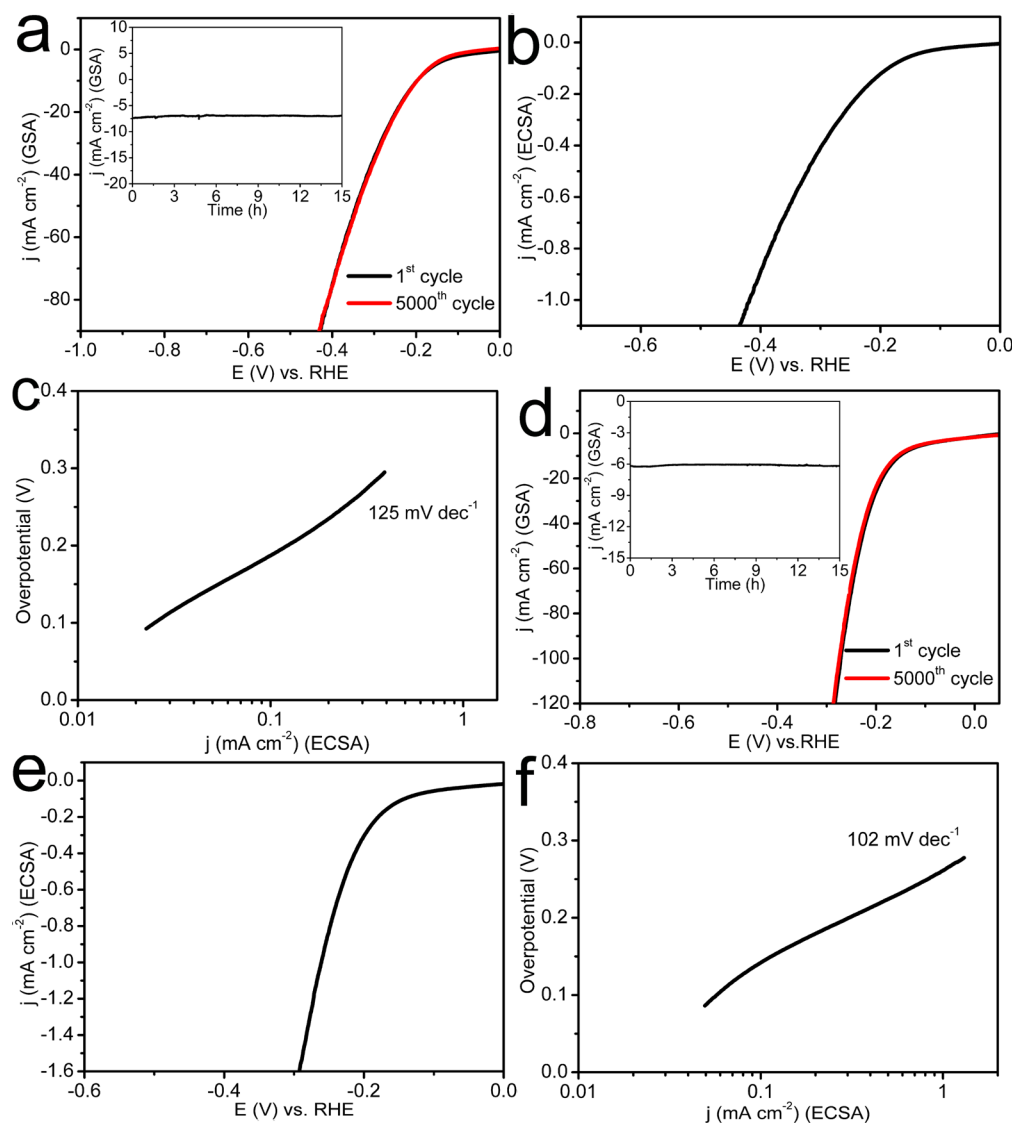
Figure 3. (a) Polarization curves for WP NAs/CC in 1.0 M PBS with a scan rate of 2 mV s^{-1} with current density normalized by GSA of the electrode (inset: time-dependent current density curve for the WP NAs/CC at an overpotential of 170 mV for 15 h). (b) Polarization curve and (c) Tafel plot for WP NAs/CC with current density normalized by ECSA in 1.0 M PBS. (d) Polarization curves for WP NAs/CC in 1.0 M KOH with a scan rate of 2 mV s^{-1} with current density normalized by GSA of the electrode (inset: time-dependent current density curve for the WP NAs/CC under static overpotential of 120 mV for 15 h). (e) Polarization curve and (f) Tafel plot for WP NAs/CC/CC with current density normalized by ECSA in 1.0 M KOH.

conditions. Figure 3d shows the polarization curve for WP NAs/CC in 1.0 M KOH (pH 14). Overpotentials of 150 and 271 mV are needed for WP NAs/CC to afford current densities of 10 and 100 mA cm^{-2}, respectively. These overpotentials also compare favorably to the behaviors of all other non-noble-metal HER catalysts in basic media except Ni−Mo alloy/Ti foil (see Table S3 in the Supporting Information). Figure 3e shows the reploted polarization curve for WP NAs/CC using the measured current normalized by the ECSA. This electrode exhibits a Tafel slope of 102 mV dec^{-1} in the region of η = 120−250 mV (Figure 3f). We further determined the Faradaic efficiency (FE) of the WP NAs/CC electrode for hydrogen evolution using reported method.[12,18,20] The agreement of the amount of experimentally quantified hydrogen with theoretically calculated hydrogen (assuming 100% FE) suggests that the FE is 100% at all pH values (Figure 4).

The excellent catalytic activity of the nanorods array at all pH values could be explained as follows: (1) WP NAs/CC guarantees intimate contact, good mechanical adhesion and electrical connection between WP CC, which facilitates electrons flowing from CC to WP. (2) The 3D configuration of WP NAs/CC allows for enhanced diffusion of protons and generated hydrogen and the exposure of more active sites. (3) The absence of polymer binder for WP NAs/CC improves the electrical conductivity of this integrated electrode on one hand,[22] and it also avoids the block of active sites and the inhibition of diffusion on the other hand.[23] Indeed, the number of active sites (n) for WP NAs/CC was determined to be nearly 1.5 times of that for WP NRs/CC (see Figure S6 in the Supporting Information) according to previously reported electrochemical method[12] and electrochemical impedance spectroscopy analysis also confirms that WP NAs/CC has much lower impedance and thus markedly faster HER kinetics than WP NRs/CC,[25] as shown in Figure S7 in the Supporting Information.
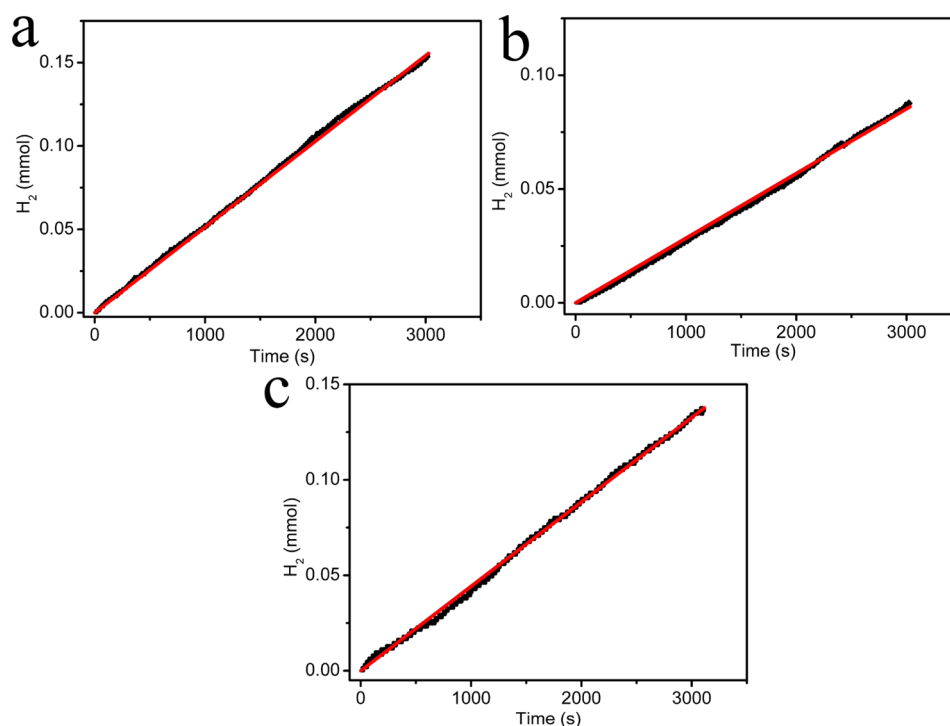
Figure 4. Amount of H_2 theoretically calculated (red line) and experimentally measured (black line) versus time for WP NAs/CC at (a) 0.5 M H_2SO_4, (b) 1 M PBS, and (c) 1 M KOH under an overpotential of 350 mV for 3000 s, respectively.
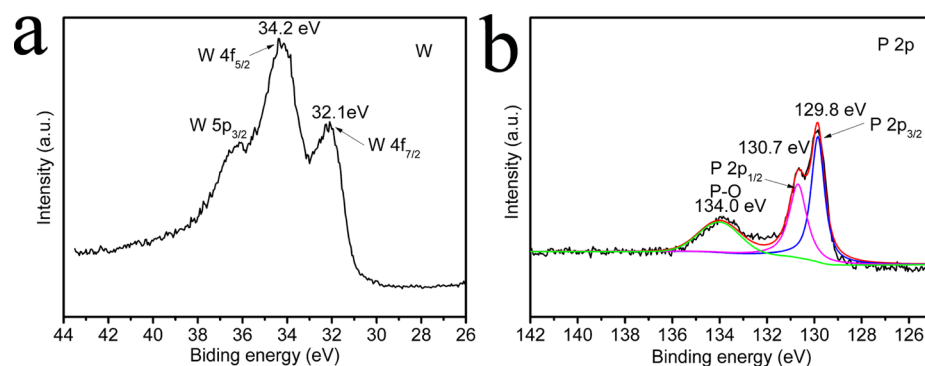
Figure 5. XPS spectra in the (a) W and (b) P regions of WP.

It is reported that both hydrogenases[26] and metal complex HER catalysts[27] incorporate proton relays from pendant acid–base groups close to the metal center where hydrogen evolution occurs. For CoP and MoP HER catalysts, they also feature pendant base P (δ^-) close proximity to the metal center M (δ^+).[12,18,20] Figure 5a, b shosw the X-ray photoelectron spectroscopy (XPS) spectra in the W and P regions for WP, respectively. Two peaks at 32.1 and 34.2 eV are assigned to W $4f_{7/2}$ and W $4f_{5/2}$, respectively. The high-resolution P(2p) region exhibits two peaks at 129.8 and 130.7 eV corresponding to the binding energy (BE) of P $2p_{3/2}$ and P $2p_{1/2}$, respectively. The predominant P species with BE of 129.8 eV can be assigned to P bonded to W while the peak at 134.0 eV is assigned to oxidized P species arising from surface oxidation due to air contact.[28] The BE of P is lower than that of elemental P (130.2 eV), whereas the BE of W is higher than that of metallic W (31.5 eV),[29] suggesting a partial positive (δ^+) and negative (δ^-) charge for W and P, respectively, and the occurrence of a small transfer of electron density from W to P in WP.[30] Based on above XPS results, we can conclude that WP

may adopt a similar catalytic mechanism toward the HER like hydrogenase, metal complex, and other TMP HER catalysts.

In summary, WP nanorod arrays have been successfully developed on CC through phosphidation of corresponding WO_3 NAs/CC precursor for the first time. When used as integrated 3D hydrogen evolution cathode, the WP NAs/CC is excellent in catalytic activity and durability at all pH values. Their electrocatalytic performance places WP NAs among the best earth-abundant alternatives to Pt catalyst toward electrochemical water splitting for large-scale hydrogen fuel production. The facile and scale-up synthesis process allows cost-effective preparation of WP or other TMPs on various conductive substrates as attractive polymer binder-free cathodes for water splitting.

■ ASSOCIATED CONTENT

Ⓢ Supporting Information

Experimental section; EDX spectrum; SEM images; XRD patterns; Tables S1−S3; ECSA calculation; CVs; exchange current density calculation; polarization curve; Tafel plot;

Nyquist plots. This material is available free of charge via the Internet at http://pubs.acs.org

■ AUTHOR INFORMATION

Corresponding Author

*E-mal: sun.xuping@hotmail.com.

Notes

The authors declare no competing financial interest.

■ REFERENCES

(1) Turner, J. A. Sustainable Hydrogen Production. *Science* **2004**, *305*, 972−974.

(2) Walter, M. G.; Warren, E. L.; McKone, J. R.; Boettcher, S. W.; Mi, Q.; Santori, E. A.; Lewis, N. S. Solar Water Splitting Cells. *Chem. Rev.* **2010**, *110*, 6446−6473.

(3) Goff, A. L.; Artero, V.; Jousselme, B.; Tran, P. D.; Guillet, N.; Métayé, R.; Fihri, A.; Palacin, S.; Fontecave, M. From Hydrogenases to Noble Metal-Free Catalytic Nanomaterials for H_2 Production and Uptake. *Science* **2009**, *326*, 1384−1387.

(4) Kong, D.; Wang, H.; Lu, Z.; Cui, Y. $CoSe_2$ Nanoparticles Grown on Carbon Fiber Paper: An Efficient and Stable Electrocatalyst for Hydrogen Evolution Reaction. *J. Am. Chem. Soc.* **2014**, *136*, 4897−4900.

(5) McKone, J. R.; Warren, E. L.; Bierman, M. J.; Boettcher, S. W.; Brunschwig, B. S.; Lewis, N. S.; Gray, H. B. Evaluation of Pt, Ni, and Ni-Mo Electrocatalysts for Hydrogen Evolution on Crystalline Si Electrodes. *Energy Environ. Sci.* **2011**, *4*, 3573−3583.

(6) Lukowski, M. A.; Daniel, A. S.; Meng, F.; Forticaux, A.; Li, L.; Jin, S. Enhanced Hydrogen Evolution Catalysis from Chemically Exfoliated Metallic MoS_2 Nanosheets. *J. Am. Chem. Soc.* **2013**, *135*, 10274−10277.

(7) Vrubel, H.; Hu, X. Molybdenum Boride and Carbide Catalyze Hydrogen Evolution in both Acidic and Basic Solutions. *Angew. Chem., Int. Ed.* **2012**, *54*, 12703−12706.

(8) Chen, W.; Sasaki, K.; Ma, C.; Frenkel, A. I.; Marinkovic, N.; Muckerman, J. T.; Zhu, Y.; Adzic, R. R. Hydrogen-Evolution Catalysts Based on Non-Noble Metal Nickel-Molybdenum Nitride Nanosheets. *Angew. Chem., Int. Ed.* **2012**, *51*, 6131−6135.

(9) Cao, B.; Veith, G. M.; Neuefeind, J. C.; Adzic, R. R.; Khalifah, P. G. Mixed Close-Packed Cobalt Molybdenum Nitrides as Non-noble Metal Electrocatalysts for the Hydrogen Evolution Reaction. *J. Am. Chem. Soc.* **2013**, *135*, 19186−19192.

(10) Kundu, A.; Sahu, J. N.; Redzwan, G.; Hashim, M. A. An Overview of Cathode Material and Catalysts Suitable for Generating Hydrogen in Microbial Electrolysis Cell. *Int. J. Hydrogen Energy* **2013**, *38*, 1745−1757.

(11) LeRoy, R. L. Industrial Water Electrolysis: Present and Future. *Int. J. Hydrogen Energy* **1983**, *8*, 401−417.

(12) Tian, J.; Liu, Q.; Asiri, A. M.; Sun, X. Self-Supported Nanoporous Cobalt Phosphide Nanowires Array: An Efficient 3D Hydrogen-Evolving Cathode Over the Wide Range 0−14 pH. *J. Am. Chem. Soc.* **2014**, *136*, 7587−7590.

(13) Zou, X.; Huang, X.; Goswami, A.; Silva, R.; Sathe, B. R.; Mikmekova, E.; Asefa, T. Cobalt-Embedded Nitrogen-Rich Carbon Nanotubes Efficiently Catalyze Hydrogen Evolution Reaction at All pH Values. *Angew. Chem., Int. Ed.* **2014**, *126*, 4372−4376.

(14) Chen, W.; Muckerman, J. T.; Fujita, E. Recent Developments in Transition Metal Carbides and Nitrides as Hydrogen Evolution Electrocatalysts. *Chem. Commun.* **2013**, *49*, 8896−8909.

(15) Chakrapani, V.; Thangala, J.; Sunkara, M. K. WO_3 and W_2N Nanowire Arrays for Photoelectrochemical Hydrogen Production. *Int. J. Hydrogen Energy* **2009**, *34*, 9050−9059.

(16) Voiry, D.; Yamaguchi, H.; Li, J.; Silva, R.; Alves, D. C. B.; Fujita, T.; Chen, M.; Asefa, T.; Shenoy, V. B.; Eda, G.; Chhowalla, M. Enhanced Catalytic Activity in Strained Chemically Exfoliated WS_2 Nanosheets for Hydrogen Evolution. *Nat. Mater.* **2013**, *12*, 850−855.

(17) Popczun, E. J.; McKone, J. R.; Read, C. G.; Biacchi, A. J.; Wiltrout, A. M.; Lewis, N. S.; Schaak, R. E. Nanostructured Nickel Phosphide as an Electrocatalyst for the Hydrogen Evolution Reaction. *J. Am. Chem. Soc.* **2013**, *135*, 9267−9270.

(18) Liu, Q.; Tian, J.; Cui, W.; Jiang, P.; Cheng, N.; Asiri, A. M.; Sun, X. Carbon Nanotubes Decorated with CoP Nanocrystals: A Highly Active Non-Noble-Metal Nanohybrid Electrocatalyst for Hydrogen Evolution. *Angew. Chem., Int. Ed.* **2014**, *53*, 6710−6714.

(19) Xu, Y.; Wu, R.; Zhang, J.; Shi, Y.; Zhang, B. Anion-Exchange Synthesis of Nanoporous FeP Nanosheets as Electrocatalysts for Hydrogen Evolution Reaction. *Chem. Commun.* **2013**, *49*, 6656−6658.

(20) Xing, Z.; Liu, Q.; Asiri, A. M.; Sun, X. Closely Interconnected Network of Molybdenum Phosphide Nanoparticles: A Highly Efficient Electrocatalyst for Generating Hydrogen from Water. *Adv. Mater.* **2014**, *26*, 5702−5707.

(21) McEnaneya, J. M.; Cromptonb, J. C.; Callejasa, J. F.; Popczuna, E. J.; Reada, C. G.; Lewis, N. S.; Schaak, R. E. Electrocatalytic Hydrogen Evolution Using Amorphous Tungsten Phosphide Nano-particles. *Chem. Commun.* **2014**, *50*, 11026−11028.

(22) Luo, Y.; Jiang, J.; Zhou, W.; Yang, H.; Luo, J.; Qi, X.; Zhang, H.; Denis, Y.; Li, C. M.; Yu, T. Self-Assembly of Well-Ordered Whisker-like Manganese Oxide Arrays on Carbon Fiber Paper and Its Application as Electrode Material for Supercapacitors. *J. Mater. Chem.* **2012**, *22*, 8634−8640.

(23) Roy-Mayhew, J. D.; Boschloo, G.; Hagfeldt, A.; Aksay, I. A. Functionalized Graphene Sheets as a Versatile Replacement for Platinum in Dye-Sensitized Solar Cells. *ACS Appl. Mater. Interfaces.* **2012**, *4*, 2794−2800.

(24) Pentland, N.; Bockris, J. O. M.; Sheldon, E. Hydrogen Evolution Reaction on Copper, Gold, Molybdenum, Palladium, Rhodium, and Iron. *J. Electrochem. Soc.* **1957**, *104*, 182−194.

(25) Guo, C.; Zhang, L.; Miao, J.; Zhang, J.; Li, C. M. DNA-Functionalized Graphene to Guide Growth of Highly Active Pd Nanocrystals as Efficient Electrocatalyst for Direct Formic Acid Fuel Cells. *Adv. Energy Mater.* **2013**, *3*, 167−171.

(26) Nicolet, Y.; de Lacey, A. L.; Vérnede, X.; Fernandez, V. M.; Hatchikian, E. C.; Fontecilla-Camps, J. C. Crystallographic and FTIR Spectroscopic Evidence of Changes in Fe Coordination upon Reduction of the Active Site of the Fe-only Hydrogenase from Desulfovibrio Desulfuricans. *J. Am. Chem. Soc.* **2001**, *123*, 1596−1601.

(27) Wilson, A. D.; Shoemaker, R. K.; Miedaner, A.; Muckerman, J. T.; Dubois, D. L.; Dubois, M. R. Nature of Hydrogen Interactions with Ni(II) Complexes Containing Cyclic Phosphine Ligands with Pendant Nitrogen Bases. *Proc. Natl. Acad. Sci. U.S.A.* **2007**, *104*, 6951−6956.

(28) Phillips, D. C.; Sawhill, S. J.; Self, R.; Bussell, M. E. Synthesis, Characterization, and Hydrodesulfurization Properties of Silica-Supported Molybdenum Phosphide Catalysts. *J. Catal.* **2002**, *207*, 266−273.

(29) *Practical Surface Analysis by Auger and X-ray Photoelectron Spectroscopy*; Briggs, D., Seah, M. P., Eds.; Wiley: New York, 1983.

(30) *Encyclopedia of Inorganic Chemistry*, 2nd ed.; King, R. B., Ed.; Wiley: Hoboken, NJ, 2005.